Composites: Part A 84 (2016) 64–75

Contents lists available at ScienceDirect

Composites: Part A

journal homepage: www.elsevier.com/locate/compositesa

Simultaneous reduction and surface functionalization of graphene oxide with wrinkled structure by diethylenetriamine (DETA) and their reinforcing effects in the flexible poly(2-ethylhexyl acrylate) (P2EHA) films

Zheng Su, Hua Wang *, Konghu Tian, Fei Xu, Weiqi Huang, Xingyou Tian *

Institute of Applied Technology, Hefei Institutes of Physical Science, Chinese Academy of Sciences, Hefei 230031, PR China

ARTICLE INFO

Article history:
Received 29 September 2015
Received in revised form 22 November 2015
Accepted 23 November 2015
Available online 28 November 2015

Keywords:
A. Graphene
A. Polymer-matrix composites (PMCs)
B. Anisotropy
C. Process modeling

ABSTRACT

NH_2-reduced graphene oxide (NH_2-rGO)/waterborne poly(2-ethylhexyl acrylate) (P2EHA) composites were prepared through an easy, all aqueous, electrostatic self-assembly method. GO was functionalized and reduced by diethylenetriamine (DETA) to achieve highly stable P2EHA/NH_2-rGO composite colloid dispersions system, leading to the formation of composites with a self-aligned layered structure and highly anisotropic properties between the direction of alignment and that perpendicular to it. The NH_2-rGO went through the structural transformation resulting in wrinkled graphene structures with many open-edge sites when N was doped into rGO sheet. The using of DETA resulted in the electrostatic interaction between the P2EHA latex and NH_2-rGO and the highly aligned, ultralarged NH_2-rGO sheets with surface wrinkles gave rise to the improved mechanical, electrical and thermal properties of the composites.

1. Introduction

Graphene, a two dimensional macromolecular sheet has sp^2-hybridized carbon atoms with a honeycomb structure, had attracted great attention in recent years owing to its outstanding thermal, mechanical, and electrical properties [1–3]. Thus, graphene sheets (GNs) were considered as an ideal nanofiller for improving thermal, mechanical, electrical, and gas barrier properties of polymers [4–8]. So far, many kinds of chemical and physical methods have been developed to avoid the aggregation of GO sheets in polymer matrices. Among these, the reduction of graphene oxide was considered as a large-scale method which was suitable for production of graphene for using as a nanofiller for polymer composite [9,10].

Graphene/polymer composites were mostly prepared through solvent mixing and in situ polymerization methods which often require a large amounts of organic solvents. Colloidal blending based on latex technology had been widely used to prepare hybrid nanocomposite particles [11]. The latex route had two major advantages as compared to the solution route or melt route. First, the aqueous medium provides a suitable environment for the reduction of GO to rGO to recover its electrical conductivity. Second, waterborne polymers were excellent candidates for achieving well-dispersed, robust and environmentally-friendly composites. With the aid of the right reagents, the interaction might develop between the graphene surface and the polymer molecules through the functional groups, such as in many carbon nanotube/polymer composites [12].

Many research focused on the interfacial properties between graphene and polymer matrix by taking graphene as a prefect flat plane. However, the graphene obtained from GO were highly wrinkled and hence could also be called "wrinkled graphenes". In addition, this wrinkled graphene could also be envisaged as viable alternatives for single layer graphene [13,14]. Graphene as a 2D material had a good potential in self-assembly into ordered structure such as lyotropic nematic liquid crystalline (LC) [15]. Above a critical concentration, GO sheets performed ordered phases as the result of the excluded volume between the ultralarge sheets. After evaporation of the solvent and combination into a solid material, the GO sheet could be transformed into layered structure [16].

However, only limited works had achieved the improvement of desired properties which was restricted by following obstacles, such as (i) agglomeration of graphene sheets in the polymer matrix, (ii) limited interfacial adhesion between the polymer and

* Corresponding authors. Tel.: +86 130 33808 1113 (H. Wang). Tel.: +86 551 65591418; fax: +86 5515591434 (X. Tian).
E-mail addresses: wanghua@issp.ac.cn (H. Wang), xytian@issp.ac.cn (X. Tian).

http://dx.doi.org/10.1016/j.compositesa.2015.11.033
1359-835X/

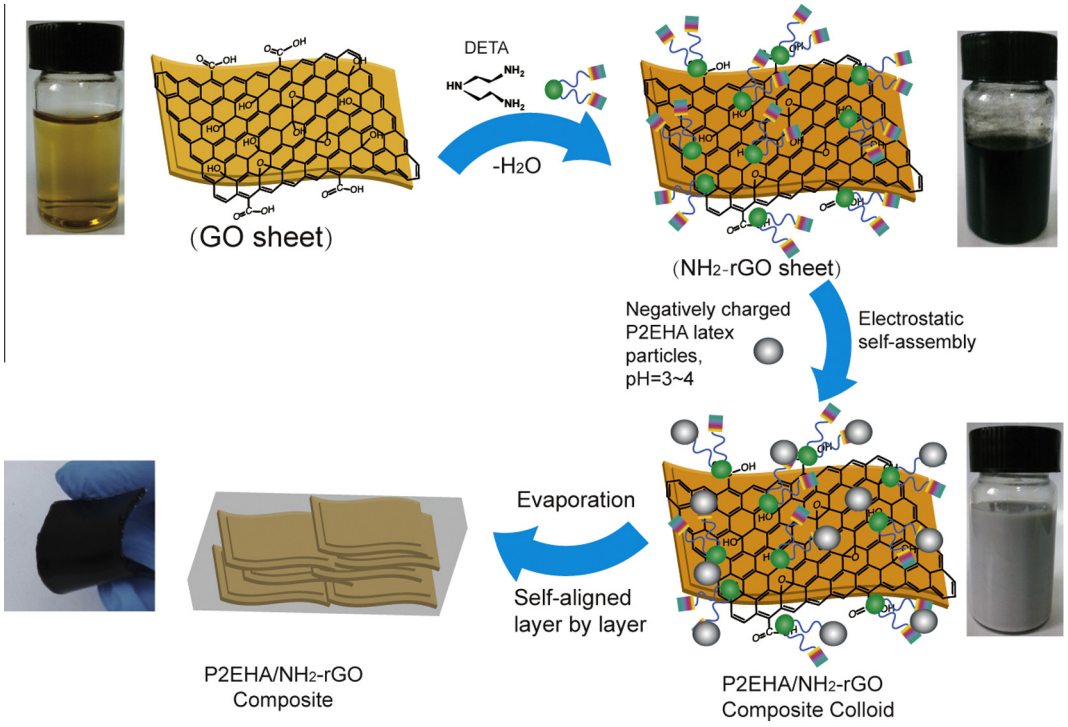

Fig. 1. Schematic illustration of the procedure used to prepare the NH_2-rGO sheet and the electrostatic self-assembly with negatively charged P2EHA latex particles and the procedure of self-aligned layer by layer. (For interpretation of the references to colour in this figure legend, the reader is referred to the web version of this article.)

graphene, and (iii) the maximum graphene level that the composites can hold to achieve the best outcome [17].

In this article, a simultaneous reduction and surface functionalization of graphene oxide by diethylenetriamine (DETA) was carried out to prepare NH_2-rGO with wrinkled structure. A simple and environmentally-friendly latex electrostatic self-assembly technology was used to fabricate aligned poly(2-ethylhexyl acrylate) (P2EHA)/graphene composite (Fig. 1). The stabilization of NH_2-rGO sheets in the presence of acrylate latex particles, in addition to the mechanical, electrical and thermal stability properties of the composites was specifically studied. A special emphasis was also placed on studying the film formation mechanisms between acrylate and rGO sheet to further elucidate the reasons behind the outstanding properties of P2EHA/NH_2-rGO composites.

2. Experimental

2.1. Preparation of graphene oxide (GO)

GO was prepared by oxidation of natural graphite powder (average area: 2025 μm^2) according to the modified Hummers' method [18]. 75 ml concentrated sulfuric acid charged into a 250 mL beaker equipped with a mechanical stirrer (Teflon impeller). The beaker was put into an ice bath to chill to 5 °C. Several grams of graphite (Qingdao Huatai Lubricant Sealing S&T Co. Ltd.) were gradually added under stirring to make a suspension. Then, 3 g $KMnO_4$ was slowly added so that the temperature did not exceed 10 °C. 2 h later, the temperature was then elevated to 35 °C, and the suspension was stirred for 24 h. The mixture was subsequently diluted with deionized water. Then, the temperature was elevated to 80 °C and kept for 2 h. 30 wt% H_2O_2 was slowly added after the temperature of mixture cooled to 30 °C. The suspension was centrifuged and washed with 1 M HCl solution four times, followed by centrifuging at 13,000 rpm and washing with deionized water to completely remove the acid until the pH of the GO dispersion reached 6. The concentration of GO was around 3.5 mg/mL, which was determined after drying the GO Dispersion at 70 °C under vacuum for 24 h.

2.2. Preparation of functional reduced graphene oxide (NH_2-rGO)

The above GO products divided into three equal parts were made up certain concentration aqueous solution. 10 wt%, 50 wt%, and 100 wt% DETA was added into each solution under vigorous stirring. The reaction continued for 24 h under reflux (80 °C). Finally, modified GO was isolated by centrifugation and throughly washed with much deionized water, filtered, and dried at 80 °C. The modified NH_2-rGO was code as 10-rGO, 50-rGO, and 100-rGO respectively.

2.3. Preparation of surface negatively charged P2EHA latex via miniemulsion polymerization

Negatively charged P2EHA latex was prepared by miniemulsion polymerization. Typically, 0.63 g SDS/Triton X-100 emulsifiers were dissolved in water to prepare the aqueous phase, and all the monomers (2-ethylhexyl acrylate: 20.70 g; acrylic acid: 0.90 g) and initiator (AIBN 0.13 g) were mixed to prepare the oil phase. As we all know that in order to avoid the Ostwald ripening effect, a costabilizer is needed. In general, the costabilizer is a low molecular weight highly water-insoluble compound, but it is unreactive and hence it will increase the volatile organic compound (VOC) content of the final latex. Therefore, in this work, the reactive monomer 2-ethylhexyl acrylate was used to minimize the Ostwald ripening effect at the same time. As it is incorporated into the polymer, it does not increase the VOC content of latex. The aqueous phase and the oil phase were added to a 250 mL glass jacketed reactor fitted with a N_2 inlet and a tetrafluoroethylene impeller rotating at 1500 rpm for 30 min. The theoretical solid content of the miniemulsion was about 45 wt%. The continuous miniemulsion

polymerization was carried out at a 250 mL glass jacketed reactor fitted with a reflux condenser, a sampling device, a N_2 inlet, a feeding inlet a tetrafluoroethylene anchor stirred equipped with two blade impellers rotating at 200 rpm. The reaction was carried out at 70 °C for 3 h, protected from light during the reaction. The latex was then cooled to below 30 °C, filtered through a 30 mesh strainer to remove the emulsion particle agglomerated.

2.4. Preparation of the P2EHA/NH_2-rGO composite film

To favor the adsorption of latex nanospheres onto the NH_2-rGO, the suspension of NH_2-rGO was added drop-by-drop to the latex placed in an ultrasonic bath. The mixture was poured in a silicone mold and dried at room temperature. The film were easily manipulated for further characterization and experiments. All the samples are code as P2EHA/X-NH_2-rGO-Y which X is the content of DETA and Y is content of NH_2-rGO. Fig. 1 shows the schematic of experimental procedures.

2.5. Characterization

Zeta potentials of the materials were measured using a zetasizer instrument (Malvern zetasizer 3000HSA). X-ray film and powder diffraction (XRD) patterns were taken on a Philips X' Pert Pro MPD X-ray diffractometer (40 kV, 40 mA) with Cu Ka radiation ($\lambda = 0.154$ nm). Measurement were done in 2θ mode using a bracket sample holder in continues mode range of 5–80° at a scan speed of 10°/min. XPS spectra were obtained via X-ray photoelec-

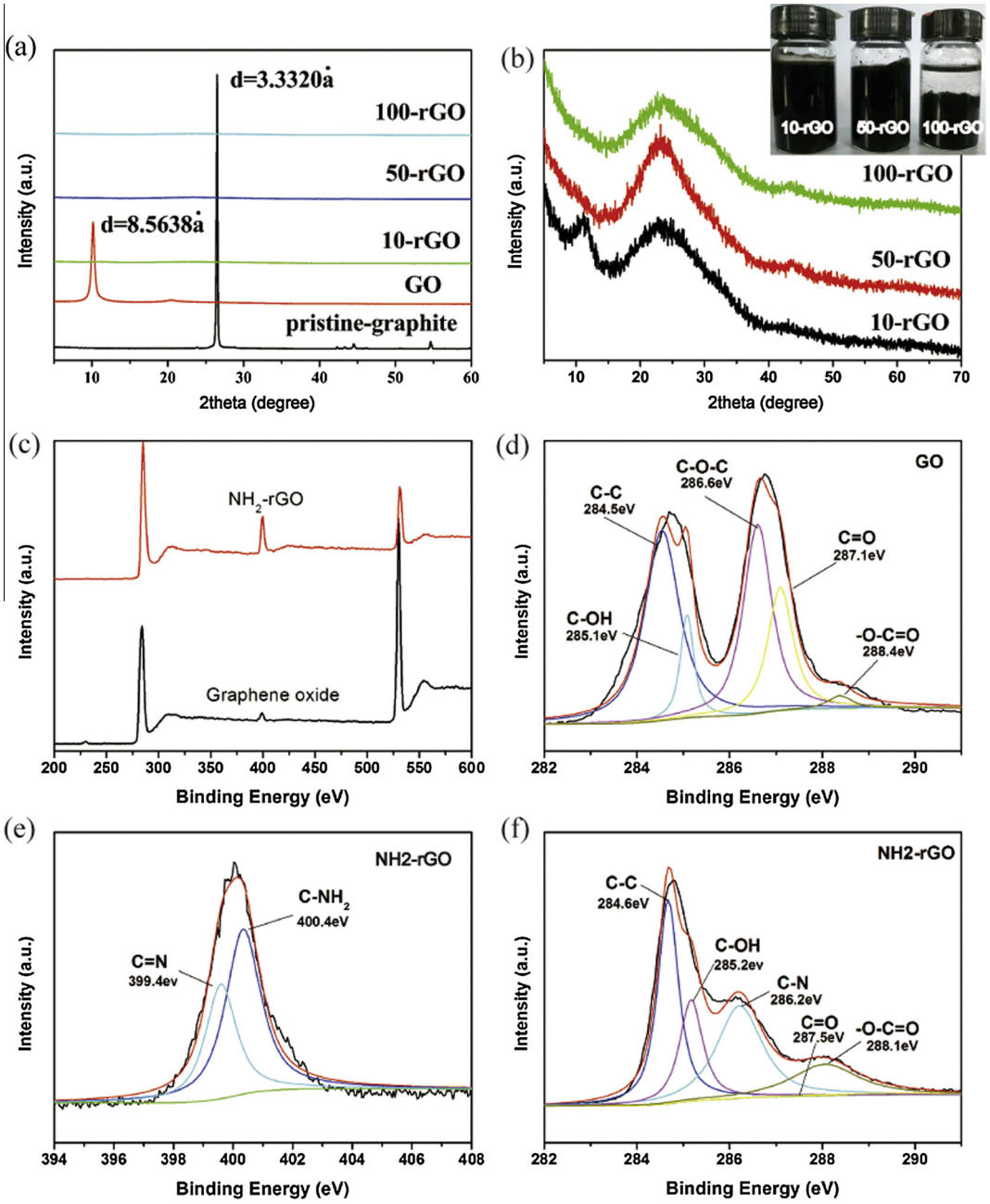

Fig. 2. (a) and (b) XRD patterns for graphite, graphene oxide and aminated graphite oxide; (c) Survey XPS spectra of GO and NH2-rGO; (d) C1s spectrum of GO; (e) N1s spectrum of NH2-rGO; (f) C1s spectrum of NH2-rGO. (For interpretation of the references to colour in this figure legend, the reader is referred to the web version of this article.)

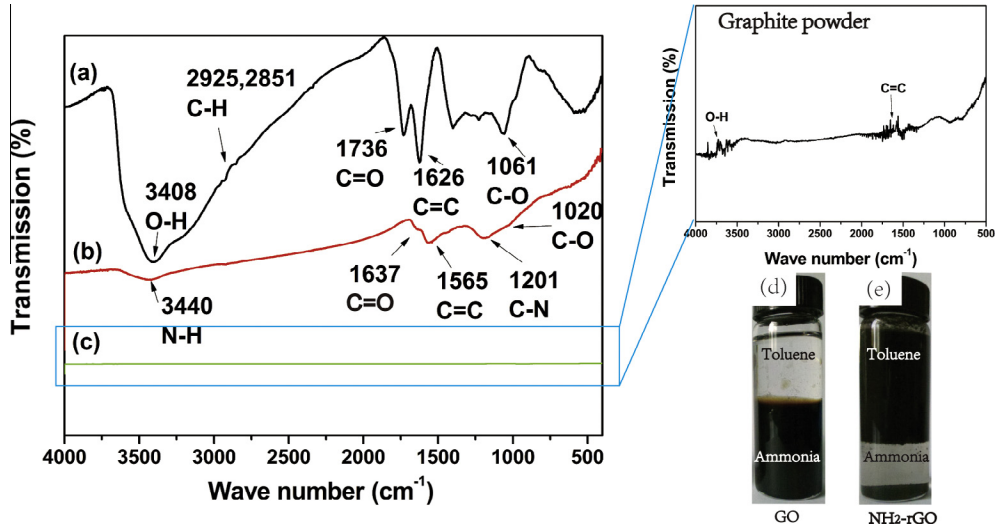

Fig. 3. IR spectra of samples (a) graphene oxide, (b) NH_2-rGO, and (c) graphite. Dispersibility comparison of (d) GO and (e) NH_2-rGO in toluene (upper layer)/ammonia solution (lower layer). (For interpretation of the references to colour in this figure legend, the reader is referred to the web version of this article.)

tron spectroscopy (American Thermo). Infrared (IR) spectra were recorded on a Nicolet 8700 FTIR spectrometer (Thermo Scientific Instrument Co. U.S.A). Raman spectra of samples were measured using a Confocal Raman Microscopy (Renishaw inVia Reflex) with an excitation wavelength of 514.5 nm. The morphologies of the composites were characterized via SEM (scanning electron microscopy) and TEM (transmission electron microscope). The software Image Tool was used to measure the areas of the individual GO sheets on SEM image. The water contact angles were measured using CAM200 contact angle goniometer, the values reported were the average of three drops per samples at different locations. Atomic force microscopic (AFM) measurements with typical tapping-mode was performed using SPA300HV AFM. Sample for AFM was prepared by dropping an aqueous GO solution (~0.01 mg/mL) onto freshly cleaved mica surfaces. Thermal properties of P2EHA/NH_2-rGO were characterized using a TGA (Q5000 IR) from 50 to 700 °C at a heating rate of 10 °C/min under nitrogen condition. ASTM D3330 Test Method A (Single-Coated Tapes, Peel Adhesion at 180° Angle) evaluated peel resistance at a peel angle of 180°. The substrate and the strip were inserted into the grips (C-clamp) and the lower grip was set to move downward at a speed of 300 mm/min. The average force per 25 mm required to peel the strip from the substrate was recorded and reported at 180°-peel resistance. ASTM D1876-01 measures T-peel resistance, akin to the test of 180°-peel resistance. Shear resistance was assessed by tension loading shear test according to ASTM D2294-96 [19] by tensile machine (CMT, SANS). This test consisted in applying a standard area of the tape (25 mm × 25 mm) on the steel panel holding in the grips (C-clamp) and the lower grip was set to move downward at a speed of 5 mm/min. All experiments were carried out under the standard conditions (T = 23 °C and humidity = 55%). With high volume resistivity beyond 10^6 Ω cm at room temperature with the size of the specimen is 50 × 25 × 1 mm^3, the high resistivity meter model LK2679A was used to measure the electrical conductivity with alignment and perpendicular direction. Data from five measurements were averaged. The bulk conductivity was calculated with the following equation [20]:

$$\sigma = L/(RS)$$

where L, R, and S are the length, resistance, and cross-sectional area of the specimen, respectively.

3. Results and discussion

3.1. Surface functionalization and reduction of GO sheet

When the NH_2-rGO sheets were added to the homogeneous dispersed P2EHA latex, adsorption of the P2EHA microspheres rapidly occurred on the surface of NH_2-rGO sheet, thereby inducing the co-coagulation of the two species [21]. As illustrated in Fig. 1, the P2EHA/NH_2-rGO composites colloid was prepared by the electrostatic interaction driven by self-assembly strategy. The electrostatic interaction which requires the two types of aqueous objects to be oppositely charged was believed to be the driving force.

The as-received P2EHA latex has been stabilized in water with the help of acrylic acid which was a auxiliary monomer commonly used in acrylate emulsion. The ionized carboxylate ions from the carboxyl groups of the acrylic acid made the as-received P2EHA particles negatively charged. GO nanosheets were negatively charged in aqueous solution, originated from the ionization of the carboxylic acid groups attached on their surface. Therefore, many researchers paid attention on GO mixed with other positively charged particles, the mutual assembly can be triggered by the electrostatic force [22]. After modification GO with DETA which formed positive charge by protonation of amino groups. After that, the abundant —NH_2 groups on the rGO surface could be protonated (—NH_3^+) in the deionized (DI) water, making them positively charged. Meanwhile, GO would be reduced to rGO. The presence of DETA prevent the aggregation of the rGO-NH^{3+} suspensions, as reported previously [23]. When the oppositely charged NH_2-rGO sheets and P2EHA particles met through a simple solution mixing, the electrostatic assembly might be triggered, forming the P2EHA/NH_2-rGO composite colloid afterward.

XRD patterns, which has been utilized as a powerful tool in the characterization of graphene and is derivative, was employed to further identify the GO, NH_2-rGO sheets and P2EHA/NH_2-rGO composite film. XRD patterns of GO and NH_2-rGO were showed in Fig. 2. Natural graphite is crystal with laminated structure. The strong and sharp diffraction peak at 2θ = 26.5° corresponds to the crystal face of graphite (002). According to Bragg law, the interplanar spacing calculated is 3.33 Å.

There was a strong peak at 2θ = 10.32° of GO, corresponding to GO (001) crystal face [24]. The interplanar spacing of GO is 8.56 Å,

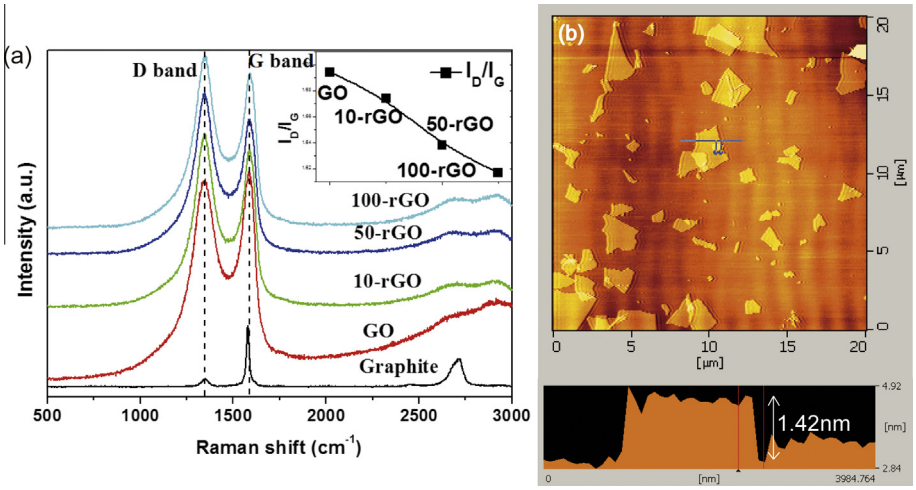

Fig. 4. (a) Raman spectra of graphite, GO, 10-rGO, 50-rGO, and 100-rGO. Small picture shows the peak area ratio of I_D and I_G of GO, 10-rGO, 50-rGO, and 100-rGO. (b) The AFM image of the GO sheets. (For interpretation of the references to colour in this figure legend, the reader is referred to the web version of this article.)

which indicates that the interaction of oxygen-containing group and water molecules makes the interplanar spacing increase.

For GO treated by DETA, there were weak and wide peaks at $2\theta = 11.55°$ and $2\theta = 23.05°$ for 10-rGO, $2\theta = 23.05°$ for 50-rGO and 100-rGO. The XRD peaks became broaden, which showed the structure of NH_2-rGO was amorphous and the rank of inner crystal plate was not nearby as regular as natural graphite. When chemical grafting created strong bonding between GO and the attached molecules, it produced additional defects on the GO surface and, hence, weakened the structure of the GO [25]. After the chemical reduction of DETA, many XPS characteristic peaks of GO are greatly weakened, shifted or disappeared, suggesting the removal of oxygen-containing groups which confirmed the efficient reduction of GO (Fig. 2). In Fig. 2(f) the additional component at 286.2 eV could be abscribed to C—N groups. In addition, it was noted that survey XPS spectra of NH_2-rGO showed the apparent nitrogen peak at ~399 eV and decreased oxygen peak at ~530 eV as compare to that of GO, which indicated the de-oxygenation or oxygen substitution by nitrogen [26,27]. This result supported the reduction and functionalization of GO by DETA. The more DETA we used the more hydroxyl group and epoxy group would be replaced. Suitable amount of DETA would result in a residual portion of the hydrophilic group and keep aminated reduced graphene oxide (NH_2-rGO) well dispersed in the aqueous phase. In sharp contrast, overmuch substitution would reduce the stability of NH_2-rGO in the aqueous phase due to the significant agglomeration (Fig. 2 the real image). So far, the irreversible aggregation of GO sheet during or after reduction had motivated many studies to find a right way to produce stable rGO dispersions [28].

The zeta potential is an important factor for characterizing the stability of colloidal dispersions and provides a measure of the magnitude and sign of the effective surface charge associated with the double layer around the colloidal particle. Generally, high value of zeta potential (positive or negative) is considered to form stable dispersions due to inter particle electrostatic repulsion. For GO the value of zeta potential is found to be −39.4 mV and for NH_2-rGO is −37.1 mV in water (pH = 6.5–7) which depicts high stability of GO and NH_2-rGO in water.

The corresponding IR spectra of samples GO and NH_2-rGO were depicted in Fig. 3. For GO, the bands presented at 1640 cm^{-1} and 1380 cm^{-1} were attributed to the deformation of the O—H bond in water and CO—H groups, respectively. The band at 1736 cm^{-1} was associated with stretching of the C=O bond of carbonyl or carboxyl groups. The intense band at 3408 cm^{-1} was attributed to stretching of the O—H bond of CO—H. Deformation of the C—O bond was observed as the intense band present at 1050–1160 cm^{-1} [26]. The peak at 2360 cm^{-1} was attributed to CO_2, which was from the decomposition of labile functional groups [29]. The IR scanning patterns of the two samples were almost the similarity with the same peaks of oxygen-containing functional groups, because of it was impossible to remove completely the oxygen-containing functional groups from the GO surface using chemical or thermal reduction, or even a combination of two. The FTIR spectra of GO intercalated with amines, as reference, differ from that of GO in signals observed at 2925 and 2851 cm^{-1}. The two peaks were assigned to the bending vibration (scissoring) of —CH_2— [30]. The acylation reaction caused the absorption of carbonyl moved from 1736 cm^{-1} to 1637 cm^{-1} due to the p–π conjugation. In all the amine intercalated samples, peaks at 3440 cm^{-1} and 1600 cm^{-1} due to N—H may coincide with O—H stretching vibrations and O—H bending vibrations [31]. The stretching vibrations of C—N was found at 1201 cm^{-1}. The weak peak of O—H and C=C was observed in the IR spectra of graphite.

The grafting of amino group on the surface of GO change the surface polarity and the dispersion in solvent (showed in Fig. 3 real image (d) and (e)). In order to verify the difference of dispersion in solvent about GO and NH_2-rGO, we dispersed them in the mixed solvent of toluene and ammonia water with the help of ultrasonic. After standing for a moment, the toluene would in the upper layer and the ammonia water would in the lower layer due to the immiscibility and density differences of them. We could find in the picture that the GO sheet tend to disperse in strongly polar solvent (ammonia) and the NH_2-rGO tend to disperse in the weak polar solvent (toluene). This meant that the amino group grafted onto the surface of GO successfully.

The structure changed from graphite to GO and NH_2-rGO were also investigated by using Raman spectroscopy. Raman spectra of samples were measured using a Confocal Raman Microscopy (Renishaw inVia Reflex) with an excitation wavelength of 514.5 nm. All samples were deposited on glass slides in powder form without using any solvent. Fig. 4 shows Raman spectra of graphite, GO, 10-rGO, 50-rGO, and 100-rGO. In the Raman spectrum of NH_2-rGO, the G-band which represented primary Raman active mode in graphite and provided a good representation of sp^2 bonded carbon that was present in planar sheet configurations with blue shift when compared GO to NH_2-rGO. The D-band (known as the disorder of defect mode that originates from disruption of planar sheet configuration at edges) was also blue shift when compared GO to

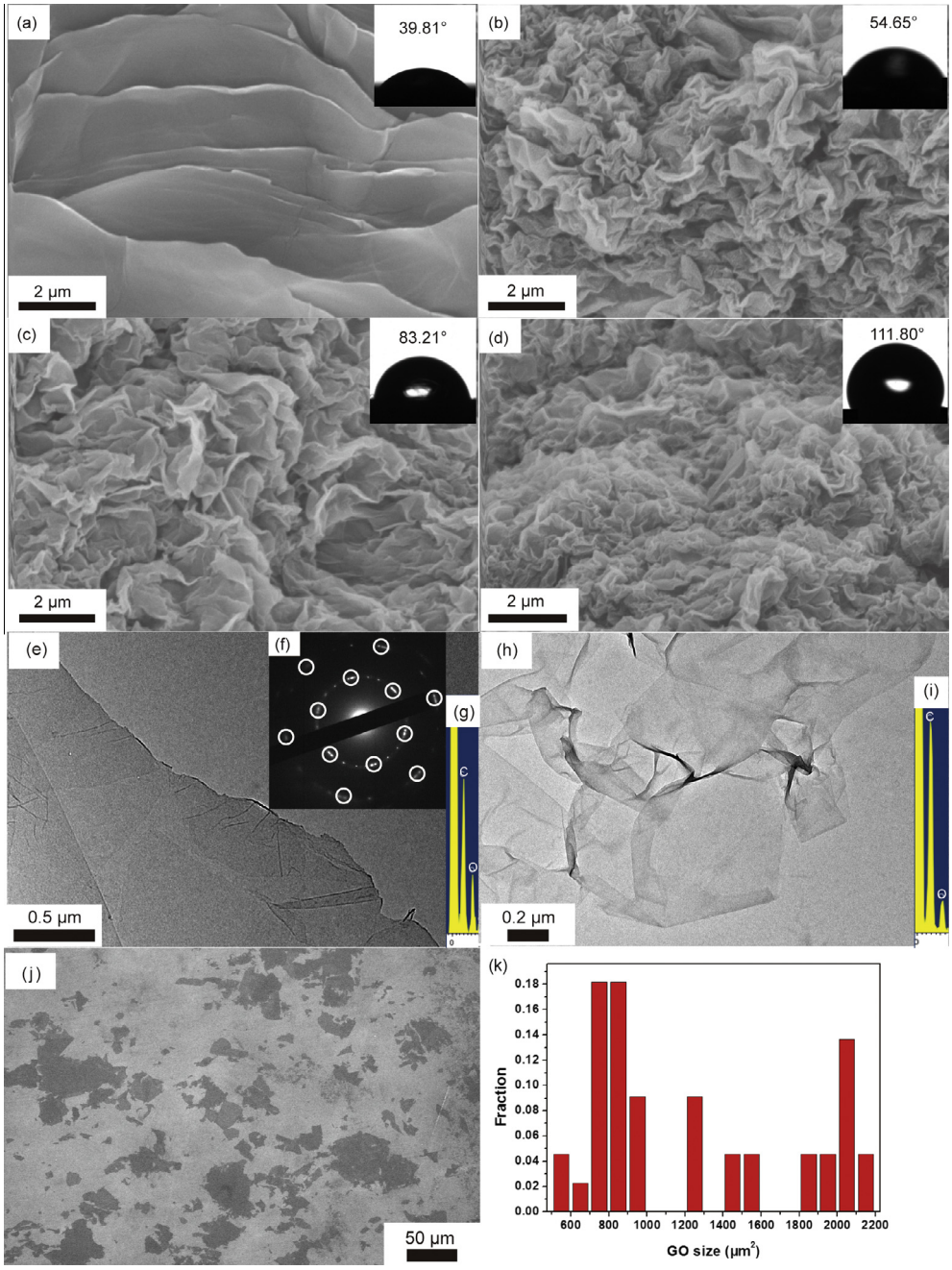

Fig. 5. SEM surface images of (a) graphene oxide, (b) 10-rGO, (c) 50-rGO, and (d) 100-rGO with the water contact angle; TEM images of (e) graphene oxide and (h) 10-rGO and (f) electron diffraction pattern of graphene oxide and the TEM–EDX pattern of (g) graphene oxide and (i) 10-rGO; (j) and (k): SEM image and area distribution of GO sheets. (For interpretation of the references to colour in this figure legend, the reader is referred to the web version of this article.)

NH_2-rGO. As it is difficult to measure absolute intensity in Raman spectroscopy, the normalized I_D/I_G ratio is used to measure the amount of disorder. Higher value of I_D/I_G meant more disorder in sample which there were more binding sites in the sample [32]. The higher values of I_D/I_G for NH_2-rGO compared to graphite indicates that the functionalization resulted in the increase in the sp^3 planar carbon atoms. But lower value of I_D/I_G of NH_2-rGO compared to GO indicated the diminution of amorphous carbons. We measured the thickness of GO sheets by AFM showed in Fig. 4(b). The thickness was around 1.42 nm which was consistent with those in previous reports, suggesting the complete exfoliation of GO sheets to individual or bilayer ones.

The amount of DETA would had significantly influence on the surface morphology of NH_2-rGO sheet. The solution of GO and NH_2-rGO were put in vacuum oven with 50 °C for 24 h, then observed. Fig. 5 shows the smooth surface of graphene oxide (GO) sheet and the wrinkles on reduced graphene oxide (rGO) sheet via SEM and TEM with water contact angle. The reducing agent of DETA destroyed the hexagonal carbon skeleton and introduced the defects (pentagon–heptagon rings) and the loss of long-range ordering on the surface of graphene sheet and then made them wrinkled [13,14]. Although the wrinkles had negative impact on mechanical and electrical properties for graphene sheets or papers [33–35], would had positive influence for polymer-matrix

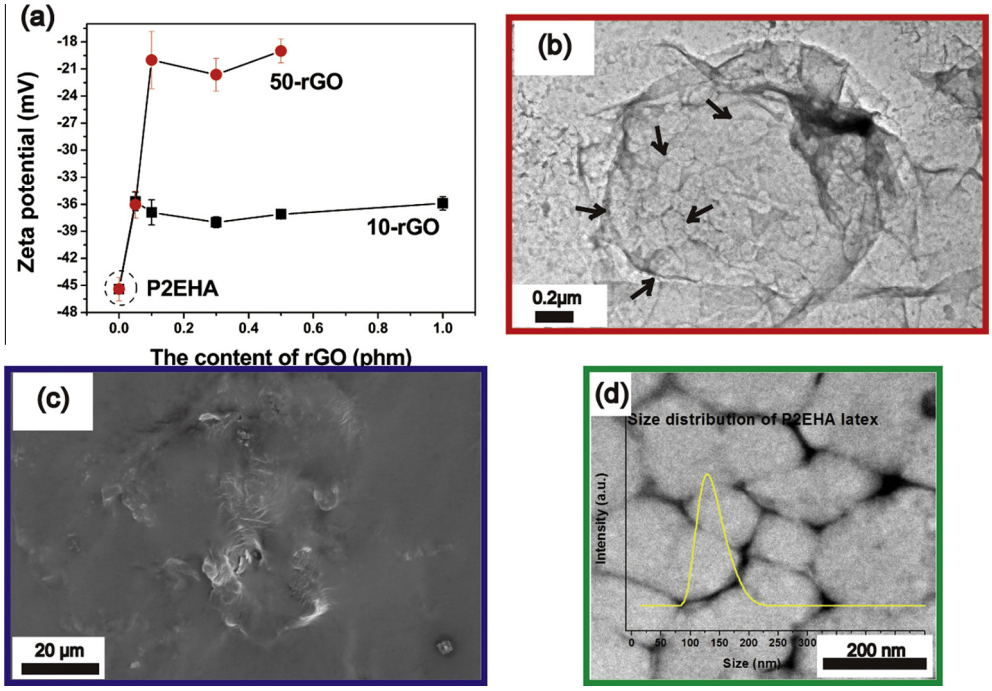

Fig. 6. (a) The zeta potential of P2EHA particle and P2EHA/NH_2-rGO composite colloid. TEM image of (b) P2EHA/10-rGO-0.05 composite colloid and (d) P2EHA latex particles with narrow size distribution, and SEM image of (c) P2EHA/10rGO-0.05 composite film's surface. (For interpretation of the references to colour in this figure legend, the reader is referred to the web version of this article.)

nano composite. The more amount of DETA we used, the more wrinkles would showed on NH_2-rGO sheet and then the hydrophilic decreased dramatically. This special morphology of NH_2-rGO sheet also revealed that the amino group located not only at the edge of NH_2-rGO sheet but also the surface which was benefit for the absorption of negatively charged particle on the surface of NH_2-rGO sheet [21].

The electron diffraction pattern of graphene oxide exhibited the typical sixfold symmetry that was expected for graphite/graphene, confirming the definitive identification of graphene in Fig. 5(g). The TEM–EDX patterns of GO and NH_2-rGO also proved the grafting of amino group on GO sheet surface and the reduction of GO with the atomic ratio of C/O increasing from 3.25 to 6.19 (Fig. 5(g) and (i)). The software Image Tool was used to measure the areas of the individual GO sheets on SEM image. Area distribution of GO sheets was showed in Fig. 5(j) and (k). The average area of GO sheet was around 1434 μm^2. Some authors define the "ultralarge" when the area of GO sheet is around 191.3 μm^2 and the reduction process will not affect the area of rGO sheets significantly.[36].

3.2. The self-assembling between ultralarge NH_2-rGO sheets and latex particles

When we mixed the P2EHA latex aqueous (pH = 3–4) and NH_2-rGO aqueous (pH = 6.5–7). Zeta potential of P2EHA/NH_2-rGO composite colloid increased due to the neutralization of positive and negative charge showed in Fig. 6(a). The more DETA we used the more N-doped sites would be found on the surface of NH_2-rGO sheet. After mixed with latex particles which would introduce to a significant decrease of zeta potential for P2EHA/rGO composite colloid. As we all know in colloidal science, suspensions with absolute zeta potential values higher than 30 mV are generally considered to be stable [37]. Therefore the stability of the composite colloid would decrease and dropped the maximum graphene level. Fig. 6(b) and (c) shows the TEM and SEM image of P2EHA/10-rGO-0.05 composite colloid. The black arrows showed the latex particles combined with graphene oxide sheet when we compared with Fig. 6(d). Therefore, we could fabricate poly(2-ethylhexyl acrylate) (P2EHA)/NH_2-rGO composite via electrostatic self-assembly approach facilely and successfully.

3.3. The film formation of P2EHA/NH_2-rGO composites film

Fig. 7 shows the XRD patterns of P2EHA/NH_2-rGO composite film. It well-know that the typical diffraction peak of NH_2-rGO (001) was observed at about $2\theta = 6.5°$, indicating an decreasing of interlayer spacing from 1.55 to 1.31 nm (Fig. 7 small picture). The diffraction peak of P2EHA was located at $2\theta = 20.1°$. When the NH_2-rGO was incorporated, the XRD of the P2EHA composites only showed the diffraction peak from P2EHA and the characteristic peak of NH_2-rGO disappears, which meant exfoliation of NH_2-rGO in the P2EHA matrix. In addition, the incorporation of NH_2-rGO increased the intensity of P2EHA, implied that incorporating NH_2-rGO increased the crystallinity of P2EHA. The increased crystallinity was probably attributed to the electrostatic interactions between P2EHA and NH_2-rGO sheets with aligned stacking could promote and strengthen the movement and arrangement of P2EHA chains [38]. Lin et al. [39] found that large-size graphene oxide (GO) sheets can impart a tremendous positive impact on self-alignment of graphene papers. The self-alignment appeared to be driven by several mechanisms, including the "excluded volume" interactions among the GO sheets of ultralarge aspect ratios, the steric hindrance between them, and gravitational force [40,41]. Other important mechanism were the interaction such as π–π stacking, van der waals forces, and electrostatic interaction acting between the adjacent GO sheets [42].

The phenomenon of self-alignment was further investigated via the confocal Raman spectroscopy and fracture surface SEM images. The composites with different NH2-rGO contents were measured with laser light along the direction of alignment and perpendicular to it. P2EHA/10-rGO-0.3 had similar Raman spectra in both directions, restating the random stacking of NH2-rGO sheets at low con-

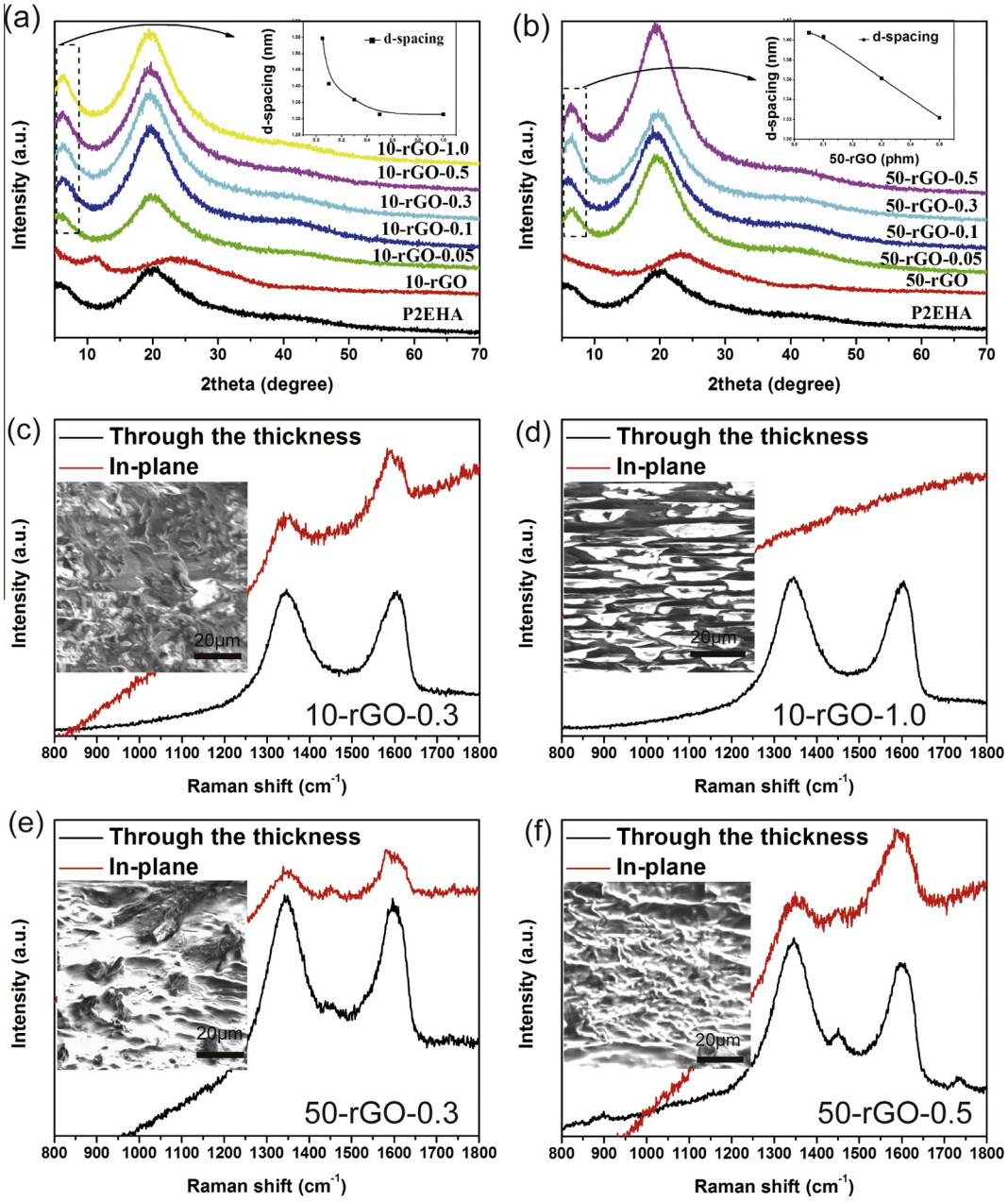

Fig. 7. (a) and (b): XRD patterns for P2EHA film, NH_2-rGO powder, and P2EHA/NH_2-rGO composite film. Small picture shows the d-spacing (001) of NH_2-rGO in polymer matrix. (c), (d), (e) and (f): Raman spectra of NH2-rGO in two directions with the fracture surface SEM images. (For interpretation of the references to colour in this figure legend, the reader is referred to the web version of this article.)

centration (Fig. 7(c)). Conversely, due to the large distance between adjacent NH2-rGO sheets, it was difficult to find more collective resonance along the in-plane direction. Therefore, P2EHA/10-rGO-1.0 showed a remarkable difference in the intensity of Raman bands in the two direction which was an evidence of self-alignment of NH2-rGO sheets (Fig. 7(d)). Because of the maximum level of 50-rGO in polymer matrix was still at low concentration, P2EHA/50-rGO-0.3 or 0.5 both had similar Raman spectra (Fig. 7 (e) and (f)). The fracture surface SEM images showed the alignment (Fig. 2(d)) and random (Fig. 2(c), (e) and (f)) structure of the composites.

Fig. 8 shows the model of the film formation mechanism of P2EHA/NH_2-rGO composite. When the ratio of P2EHA latex particle and NH_2-rGO sheet was high, the excess of P2EHA latex particle would not absorb on the surface of NH_2-rGO sheet and prevented the aligned stacking of NH_2-rGO sheets (Fig. 8 (a)). Excessively low ratio would introduce to the phase separation due to the poor compatibility (Fig. 8(c)). Suitable ratio led to the aligned stacking of NH_2-rGO sheets due to the assistance by latex particles (Fig. 8(b)).

One of the obstacles which limited to achieved the improvement of desired properties for composites was that the maximum graphene level that the composites can hold to achieve the best outcome. The wrinkled morphology of the NH_2-rGO is the results of reduction process by DETA [17]. The more DETA we used the poorer hydrophilicity and stability for NH_2-rGO and composite colloid would present which supported by water contact angle (Fig. 5) and zeta potential of composite colloid (Fig. 6). Therefore the maximum graphene level (concentration of NH_2-rGO sheets) will also be affected and then influence the alignment of graphene sheet in polymer matrix (Fig. 8).

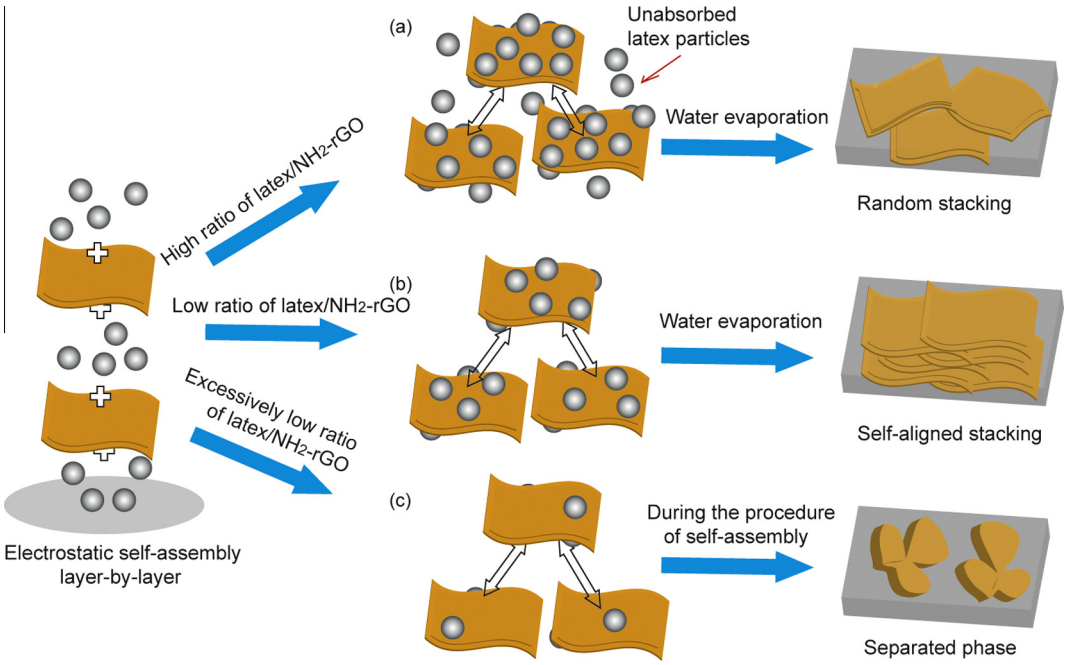

Fig. 8. The film formation mechanism of P2EHA/NH_2-rGO composite through adjusting the ratio of latex/NH_2-rGO. (For interpretation of the references to colour in this figure legend, the reader is referred to the web version of this article.)

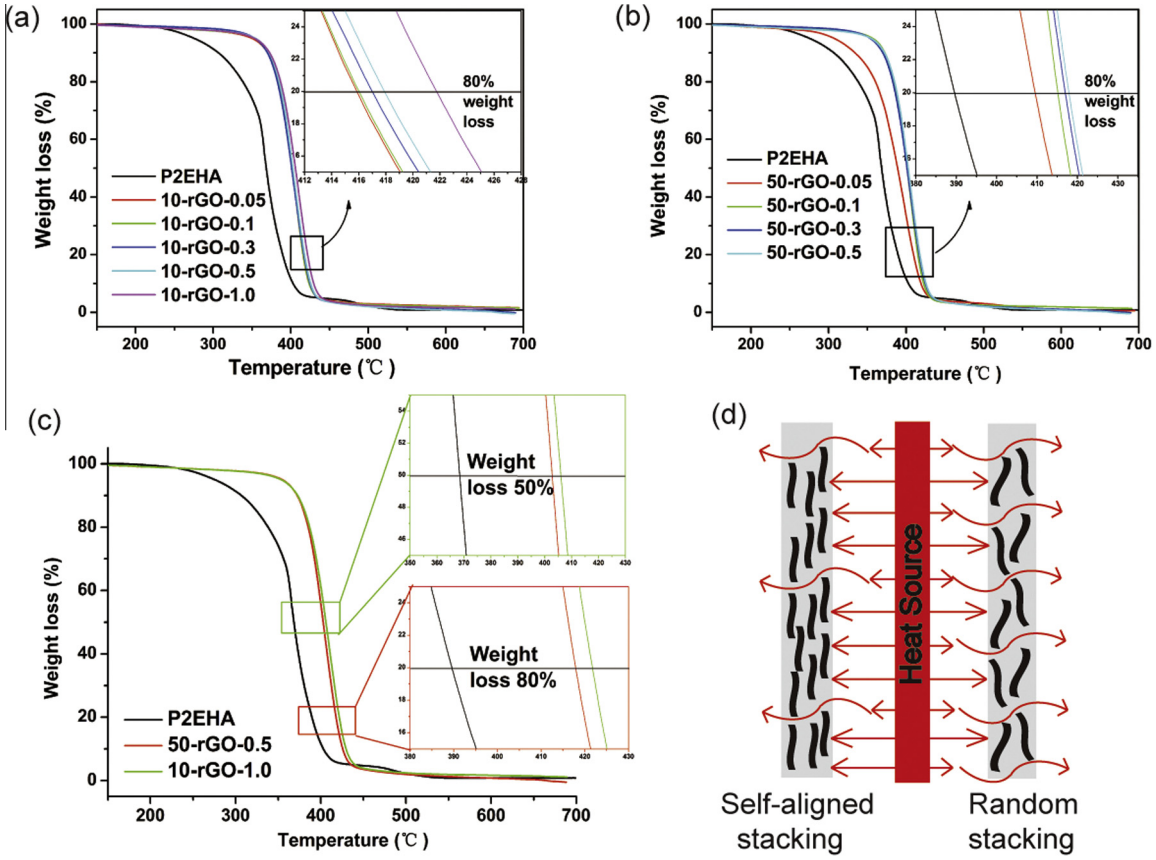

Fig. 9. Thermal stability of P2EHA/NH_2-rGO composites (a), (b) and (c). The model of thermal tolerance performance (d). (For interpretation of the references to colour in this figure legend, the reader is referred to the web version of this article.)

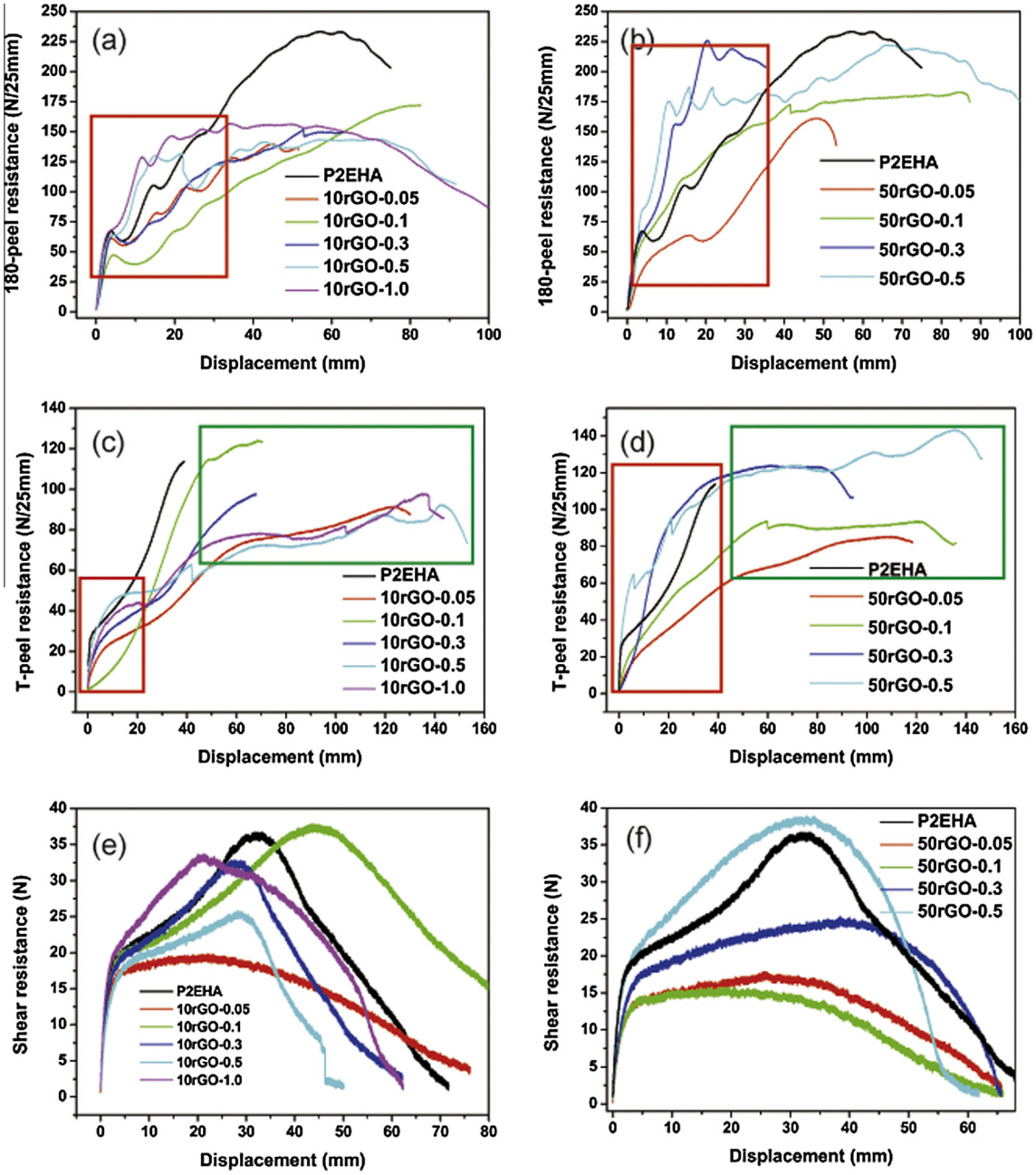

Fig. 10. The effect of NH_2-rGO concentration on adhesion properties, (a) and (b) 180°-peel, (c) and (d) T-peel and (e) and (f) shear resistance. (For interpretation of the references to colour in this figure legend, the reader is referred to the web version of this article.)

3.4. Thermal stability of the composite film

The thermal stability of P2EHA/NH_2-rGO composites was characterized in nonoxidative condition by TGA is shown in Fig. 9. There are a very negligible trace of water in the composites, confirming the complete evaporation of moisture due to curing at a high temperature. The maximum level of 50-rGO is 0.5 phm and the maximum level of 10-rGO is 1.0 wt.% which represent the best outcome respectively. However, the P2EHA/10rGO-1.0 is self-aligned stacking with filler network structure but P2EHA/50rGO-0.5 is random stacking that the filler cannot penetrate the polymer matrix (Fig. 7). The addition of NH_2-rGO also had a negligible effect on the onset of decomposition (T_{onset}) of the composites. Nevertheless, they had some tangible influences on 50% weight loss ($T_{50\%}$) and 80% weight loss ($T_{80\%}$) that the P2EHA/10-rGO (self-aligned stacking) showing about 3~4 °C higher than the P2EHA/50-rGO (random stacking) and both about 26–32 °C higher than the puer P2EHA with reduced the decomposition rate, possibly due to the formation of a high aspect ratio, inflammable NH_2-rGO stacked structure in the polymer matrix, which act a barrier inhibiting the emission of the decomposition product during combustion (Fig. 9(d)) [43,44].

3.5. Adhesive properties

Interfacial mechanical properties between nanofiller and polymer matrix were extremely important for various nanocomposites. Liu et al. [45] investigated the interfacial mechanical properties of polymer nanocomposites reinforced by wrinkled graphene via molecular dynamics (MD) simulations with a result that the wrin-

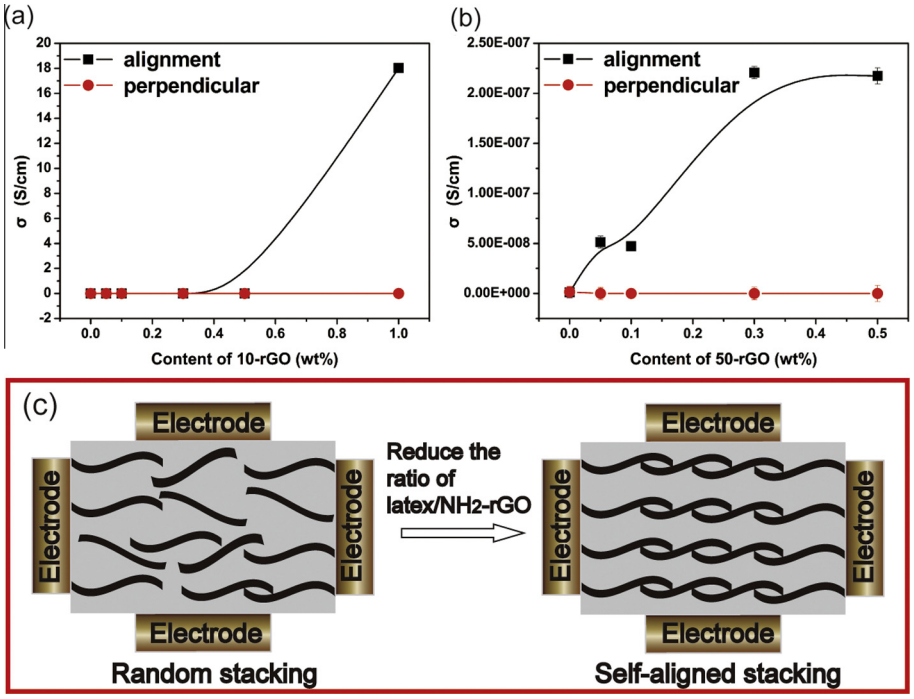

Fig. 11. (a) and (b) Electrical conductivity of P2EHA/NH_2-rGO composites with direction of alignment and perpendicular. (c) Conductive network model with adjusting the ratio of latex/NH_2-rGO. (For interpretation of the references to colour in this figure legend, the reader is referred to the web version of this article.)

kles of graphene caused the remarkable increase of interfacial mechanical properties especially for acrylate (PMMA) system. Because one of the most common applications of P2EHA was as adhesive [46], we tested the effect of loading graphene oxide on the adhesive properties of P2EHA. Fig. 10 shows the adhesion properties of the P2EHA/NH_2-rGO composites. It was worth noting that the adhesive properties was mostly due to increases in displacement at failure on addition of NH2-rGO sheet. A much little but significant increase in the 180°-peel resistance, T-peel resistance was observed with high loading levels (Fig. 10 [1]red box). Longer displacement than pure P2EHA shows the improvement of cohesive with loading of NH_2-rGO (Fig. 10 green box). This showed that reduced graphene oxide addition could have a positive effect on adhesive properties of P2EHA. The graphene with wrinkles has high surface area makes the strong interfacial interactions between polymer chains and the graphene oxide surface and causes the remarkable increase of interfacial mechanical properties [47]. Under stress, the cavities begin to form in the adhesive. When failure in cohesive, these cavities tend to be wholly appeared within the adhesive. Once the cavity formed, the stress is maintained by fibrils in a process similar to crack in polymer [48]. As the displacement was increased the cavities expanded and the fibrils became extended. This process dissipates considerable amounts of energy, often resulting in high adhesive resistance. Failure occurred when the last fibrils break which resulted in the decreasing of adhesive resistance compared with pure P2EHA.

3.6. Conductivity characteristics of P2EHA/NH_2-rGO composite film

Poor conductivity of GO was due to conjugated structure breaking during the chemical process. The improved conductivity of NH_2-rGO was obviously due to the functionalization effect of amine groups which donate electron density to aromatic rings of graphene and restored the conjugated structure partially [26]. Polymer composites appeared a rapid transition from insulator to conductor when the filler content surpassed a percolation threshold as a result of the formation of 3D networks in polymer matrix [49]. In Fig. 11(c), while the NH_2-rGO sheets cannot penetrate the P2EHA matrix, a network of NH_2-rGO sheets would remain in the composites. This graphene network would form conductive pathways in the alignment of NH_2-rGO sheets, loading to an improved conductive property. In Fig. 11(a), a further increasing in 10-rGO content beyond 1 phm resulted in a rather saturated conductivity with a remarkable value above 18 S/cm that was high enough for many practical applications including antistatic coatings [50], electromagnetic interference (EMI) shields [36]. However, we could easily find that the limited maximum graphene level that the composites can hold restricted the best outcome.

Another interesting finding from Fig. 11(a) and (b) was that the conductivities of the composites along the alignment direction and that perpendicular to it revealing a remarkable difference between the two direction as the result of the anisotropic, aligned structure. This funding further signified better alignment with increasing NH_2-rGO content. As the result, the electrical contact was well maintained between the adjacent conductive NH_2-rGO sheets along the alignment direction whereas there was less contact between the NH_2-rGO sheets in the perpendicular direction showed in Fig. 11(c). A similar difference in conductivity had also been reported for aligned graphene or CNT/epoxy composites [51–53].

4. Conclusion

In this study, PEHA/NH_2-rGO composites were prepared by directly mixing negatively charged P2EHA latex and positively charged NH_2-rGO in water through electrostatic interaction, followed by solvent evaporation. The P2EHA latex particles are assembled on the surface of the NH_2-rGO surface to form a uniform dispersion in polymer matrix. Reinforced thermal stability, adhesive properties and electrical conductivity we obtained. However,

[1] For interpretation of color in Fig. 10, the reader is referred to the web version of this article.

there are still some problems we have to overcome, such as the maximum graphene level that the composites can hold to achieve the best outcome. Through the combination of latex technology and assembly strategy, an effective and environmentally friendly method, without complicated chemical functionalization reactions and extensive toxic organic agents' use, has been developed to fabricate electrically conductive P2EHA/NH_2-rGO composites with improved dispersion uniformity and controllable structure. This strategy can be anticipated to provide a platform to prepare polymer/graphene composites with high performance and multifunctionality for potential application in various areas.

Acknowledgments

Senior Engineer Zhaoqin Chu is acknowledged for TEM assistance and Dr. Wei Xu is thanked for the TGA studies from Institute of Solid State Physics, CAS.

References

[1] Geim AK, Novoselov KS. The rise of graphene. Nat Mater 2007;6(3):183–91.
[2] Wang T, Lei CH, Dalton AB, Creton C, Lin Y, Fernando KAS, et al. Waterborne, nanocomposite pressure-sensitive adhesives with high tack energy, optical transparency, and electrical conductivity. Adv Mater 2006;18(20):2730–4.
[3] Geim AK. Graphene: status and prospects. Science 2009;324(5934):1530–4.
[4] Yoonessi M, Gaier JR. Highly conductive multifunctional graphene polycarbonate nanocomposites. ACS Nano 2010;4(12):7211–20.
[5] Potts JR, Lee SH, Alam TM, An J, Stoller MD, Piner RD, et al. Thermomechanical properties of chemically modified graphene/poly(methyl methacrylate) composites made by in situ polymerization. Carbon 2011;49(8):2615–23.
[6] Song W-L, Cao M-S, Lu M-M, Bi S, Wang C-Y, Liu J, et al. Flexible graphene/polymer composite films in sandwich structures for effective electromagnetic interference shielding. Carbon 2014;66:67–76.
[7] Choi J-Y, Kim SW, Cho KY. Improved thermal conductivity of graphene encapsulated poly(methyl methacrylate) nanocomposite adhesives with low loading amount of graphene. Compos Sci Technol 2014;94:147–54.
[8] Jiao W, Shioya M, Wang R, Yang F, Hao L, Niu Y, et al. Improving the gas barrier properties of Fe_3O_4/graphite nanoplatelet reinforced nanocomposites by a low magnetic field induced alignment. Compos Sci Technol 2014;99:124–30.
[9] Bai H, Li C, Shi G. Functional composite materials based on chemically converted graphene. Adv Mater 2011;23(9):1089–115.
[10] Zhang J, Yang H, Shen G, Cheng P, Zhang J, Guo S. Reduction of graphene oxide via L-ascorbic acid. Chem Commun 2010;46(7):1112–4.
[11] Tkalya E, Ghislandi M, Alekseev A, Koning C, Loos J. Latex-based concept for the preparation of graphene-based polymer nanocomposites. J Mater Chem 2010;20(15):3035–9.
[12] Maiti S, Shrivastava NK, Suin S, Khatua BB. Polystyrene/MWCNT/graphite nanoplate nanocomposites: efficient electromagnetic interference shielding material through graphite nanoplate–MWCNT–graphite nanoplate networking. ACS Appl Mater Interfaces 2013;5(11):4712–24.
[13] Kaniyoor A, Baby TT, Arockiadoss T, Rajalakshmi N, Ramaprabhu S. Wrinkled graphenes: a study on the effects of synthesis parameters on exfoliation–reduction of graphite oxide. J Phys Chem C 2011;115(36):17660–9.
[14] Wei YJ, Wu JT, Yin HQ, Shi XH, Yang RG, Dresselhaus M. The nature of strength enhancement and weakening by pentagon–heptagon defects in graphene. Nat Mater 2012;11(9):759–63.
[15] Aboutalebi SH, Gudarzi MM, Zheng QB, Kim J-K. Spontaneous formation of liquid crystals in ultralarge graphene oxide dispersions. Adv Funct Mater 2011;21(15):2978–88.
[16] Yousefi N, Gudarzi MM, Zheng Q, Aboutalebi SH, Sharif F, Kim J-K. Self-alignment and high electrical conductivity of ultralarge graphene oxide–polyurethane nanocomposites. J Mater Chem 2012;22(25):12709–17.
[17] Yousefi N, Sun X, Lin X, Shen X, Jia J, Zhang B, et al. Highly aligned graphene/polymer nanocomposites with excellent dielectric properties for high-performance electromagnetic interference shielding. Adv Mater 2014;26(31):5480–7.
[18] Hummers WS, Offeman RE. Preparation of graphitic oxide. J Am Chem Soc 1958;80(6). 1339–1339.
[19] Kobayashi M, Takahara A. Environmentally friendly repeatable adhesion using a sulfobetaine-type polyzwitterion brush. Polym Chem 2013;4(18):4987–92.
[20] Liu K, Chen L, Chen Y, Wu J, Zhang W, Chen F, et al. Preparation of polyester/reduced graphene oxide composites via in situ melt polycondensation and simultaneous thermo-reduction of graphene oxide. J Mater Chem 2011;21(24):8612–7.
[21] Liang J, Xu Y, Huang Y, Zhang L, Wang Y, Ma Y, et al. Infrared-triggered actuators from graphene-based nanocomposites. J Phys Chem C 2009;113(22):9921–7.
[22] Hong J, Char K, Kim B-S. Hollow capsules of reduced graphene oxide nanosheets assembled on a sacrificial colloidal particle. J Phys Chem Lett 2010;1(24):3442–5.
[23] Li D, Muller MB, Gilje S, Kaner RB, Wallace GG. Processable aqueous dispersions of graphene nanosheets. Nat Nanotechnol 2008;3(2):101–5.
[24] Liu J, Jeong H, Liu J, Lee K, Park J-Y, Ahn YH, et al. Reduction of functionalized graphite oxides by trioctylphosphine in non-polar organic solvents. Carbon 2010;48(8):2282–9.
[25] Hsiao MC, Liao SH, Yen MY, Liu PI, Pu NW, Wang CA, et al. Preparation of covalently functionalized graphene using residual oxygen-containing functional groups. ACS Appl Mater Interfaces 2010;2(11):3092–9.
[26] Lai L, Chen L, Zhan D, Sun L, Liu J, Lim SH, et al. One-step synthesis of NH2-graphene from in situ graphene-oxide reduction and its improved electrochemical properties. Carbon 2011;49(10):3250–7.
[27] Chen Y, Wang Y, Zhang H-B, Li X, Gui C-X, Yu Z-Z. Enhanced electromagnetic interference shielding efficiency of polystyrene/graphene composites with magnetic Fe_3O_4 nanoparticles. Carbon 2015;82:67–76.
[28] Gudarzi MM, Sharif F. Characteristics of polymers that stabilize colloids for the production of graphene from graphene oxide. J Colloid Interface Sci 2010;349(1):63–9.
[29] Schniepp HC, Li JL, McAllister MJ, Sai H, Herrera-Alonso M, Adamson DH, et al. Functionalized single graphene sheets derived from splitting graphite oxide. J Phys Chem B 2006;110(17):8535–9.
[30] Acik M, Lee G, Mattevi C, Chhowalla M, Cho K, Chabal YJ. Unusual infrared-absorption mechanism in thermally reduced graphene oxide. Nat Mater 2010;9(10):840–5.
[31] Yang A, Li J, Zhang C, Zhang W, Ma N. One-step amine modification of graphene oxide to get a green trifunctional metal-free catalyst. Appl Surf Sci 2015;346:443–50.
[32] Jorio A. Raman spectroscopy in graphene-based systems: prototypes for nanoscience and nanometrology. ISRN Nanotechnol 2012:1.
[33] Shen X, Lin X, Yousefi N, Jia J, Kim J-K. Wrinkling in graphene sheets and graphene oxide papers. Carbon 2014;66:84–92.
[34] Zhang J, Zhao J, Lu J. Intrinsic strength and failure behaviors of graphene grain boundaries. ACS Nano 2012;6(3):2704–11.
[35] Zhu W, Low T, Perebeinos V, Bol AA, Zhu Y, Yan H, et al. Structure and electronic transport in graphene wrinkles. Nano Lett 2012;12(7):3431–6.
[36] Yousefi N, Lin X, Zheng Q, Shen X, Pothnis JR, Jia J, et al. Simultaneous in situ reduction, self-alignment and covalent bonding in graphene oxide/epoxy composites. Carbon 2013;59:406–17.
[37] van Ravensteijn BG, Kegel WK. Colloids with continuously tunable surface charge. Langmuir 2014;30(35):10590–9.
[38] Gedler G, Antunes M, Velasco JI. Graphene-induced crystallinity of bisphenol A polycarbonate in the presence of supercritical carbon dioxide. Polymer 2013;54(23):6389–98.
[39] Lin X, Shen X, Zheng Q, Yousefi N, Ye L, Mai Y-W, et al. Fabrication of highly-aligned, conductive, and strong graphene papers using ultralarge graphene oxide sheets. ACS Nano 2012;6(12):10708–19.
[40] Lyatskaya Y, Balazs AC. Modeling the phase behavior of polymer-clay composites. Macromolecules 1998;31(19):6676–80.
[41] Ansari S, Kelarakis A, Estevez L, Giannelis EP. Oriented arrays of graphene in a polymer matrix by in situ reduction of graphite oxide nanosheets. Small 2010;6(2):205–9.
[42] Yousefi N, Gudarzi MM, Zheng Q, Lin X, Shen X, Jia J, et al. Highly aligned, ultralarge-size reduced graphene oxide/polyurethane nanocomposites: mechanical properties and moisture permeability. Compos Part A: Appl Sci Manuf 2013;49:42–50.
[43] Kim H, Abdala AA, Macosko CW. Graphene/polymer nanocomposites. Macromolecules 2010;43(16):6515–30.
[44] Kuila T, Bose S, Hong CE, Uddin ME, Khanra P, Kim NH, et al. Preparation of functionalized graphene/linear low density polyethylene composites by a solution mixing method. Carbon 2011;49(3):1033–7.
[45] Liu F, Hu N, Ning H, Liu Y, Li Y, Wu L. Molecular dynamics simulation on interfacial mechanical properties of polymer nanocomposites with wrinkled graphene. Comput Mater Sci 2015;108(Part A):160–7.
[46] Foster AB, Lovell PA, Rabjohns MA. Control of adhesive properties through structured particle design of water-borne pressure-sensitive adhesives. Polymer 2009;50(7):1654–70.
[47] Yang J, Bai L, Feng G, Yang X, Lv M, Ca Zhang, et al. Thermal reduced graphene based poly(ethylene vinyl alcohol) nanocomposites: enhanced mechanical properties, gas barrier, water resistance, and thermal stability. Ind Eng Chem Res 2013;52(47):16745–54.
[48] William D, Callister DGR. Materials science and engineering: an introduction. 7th ed. New York: Wiley; 2007.
[49] Li J, Ma PC, Chow WS, To CK, Tang BZ, Kim JK. Correlations between percolation threshold, dispersion state, and aspect ratio of carbon nanotubes. Adv Funct Mater 2007;17(16):3207–15.
[50] Wang H, Xie G, Fang M, Ying Z, Tong Y, Zeng Y. Electrical and mechanical properties of antistatic PVC films containing multi-layer graphene. Compos Part B: Eng 2015;79:444–50.
[51] Wang Q, Dai J, Li W, Wei Z, Jiang J. The effects of CNT alignment on electrical conductivity and mechanical properties of SWNT/epoxy nanocomposites. Compos Sci Technol 2008;68(7–8):1644–8.
[52] Wu S, Ladani RB, Zhang J, Bafekrpour E, Ghorbani K, Mouritz AP, et al. Aligning multilayer graphene flakes with an external electric field to improve multifunctional properties of epoxy nanocomposites. Carbon 2015;94:607–18.
[53] Wang Z, Shen X, Akbari Garakani M, Lin X, Wu Y, Liu X, et al. Graphene aerogel/epoxy composites with exceptional anisotropic structure and properties. ACS Appl Mater Interfaces 2015;7(9):5538–49.